

Article

Development of a Musculoskeletal Model of Hyolaryngeal Elements for Understanding Pharyngeal Swallowing Mechanics

Takuya Hashimoto ^{1,*} , Mariko Urabe ¹, Foo Chee-Sheng ¹, Atsuko Murakoshi ², Takahiro Kikuchi ³, Yukihiro Michiwaki ³ and Takuji Koike ²

¹ Department of Mechanical Engineering, Tokyo University of Science, Tokyo 125-8585, Japan; urabe322415@hassylab.com (M.U.); c.sheng0210@gmail.com (F.C.-S.)

² Department of Mechanical Engineering and Intelligent Systems, The University of Electro-Communications, Tokyo 182-8585, Japan; atsuko.murakoshi@shi-g.com (A.M.); koike@mce.uec.ac.jp (T.K.)

³ Japanese Red Cross Musashino Hospital, Tokyo 180-8610, Japan; oralsurg@musashino.jrc.or.jp (T.K.); yukirom@musashino.jrc.or.jp (Y.M.)

* Correspondence: tak@rs.tus.ac.jp

Received: 14 August 2020; Accepted: 7 September 2020; Published: 9 September 2020



Featured Application: The potential application of this study is to provide a key tool to help researchers and clinicians understand how neuro, muscular, and skeletal systems are involved in swallowing. It would contribute to the clinical decision-making process in treating dysphagia associated with neuromuscular disease.

Abstract: A detailed understanding of muscle activity in human swallowing would provide insights into the complex neuromuscular coordination underlying swallowing. The purpose of this study was to introduce musculoskeletal analysis to investigate muscle activities involved in swallowing as there are limitations on studying comprehensive muscle activation patterns by conventional methods such as electromyography (EMG) measurement. A musculoskeletal model of swallowing was newly developed based on the skeletal model made from CT data of a healthy volunteer. Individual muscle forces were predicted in pharyngeal swallowing by inverse dynamics' computations with static optimization, in which the typical trajectories of the hyoid bone and thyroid cartilage analyzed from videofluoroscopic (VF) data of the volunteer were used. The results identified the contribution of individual muscles in pharyngeal swallowing in relation to the movements of the hyoid bone and thyroid cartilage. The predicted sequence of muscle activity showed a qualitative agreement with salient features in previous studies with fine wire EMG measurements. This method, if validated further by imaging and EMG studies, enables studying a broader range of neuromuscular coordination in swallowing. The proposed method offers an avenue to understanding the physiological mechanisms of swallowing and could become useful to evaluate rehabilitation effects on dysphagia.

Keywords: deglutition; musculoskeletal model; muscle activity; simulation; swallowing biomechanics

1. Introduction

The increase in the number of aged in the Japanese population is faster than any other country and the elderly (aged 65 or over) comprised 27.3% in 2016 [1]. One critical issue accompanying aging is impairment of physical and cognitive abilities, with the decline in the ability to swallow particularly causing serious problems including aspiration pneumonia. Therefore, dysphagia difficulty with swallowing is a serious health concern in an aging society, and pneumonia has been the third most common cause of death in Japan from 2011 [2], with most of the pneumonia in the elderly ascribed to

aspiration pneumonia caused by dysphagia [3,4]. Disability in swallowing also increases the risks of suffocation, undernutrition, and dehydration, which have the potential to decrease the quality of life. Therefore, prevention and treatment of dysphagia are a social issue in an aging society with extended healthy life spans and social welfare concerns.

Swallowing, or deglutition, is a coordinated and smoothly functioning process to propel food and drink from the mouth to the esophagus. Since it involves complex neuromuscular coordination [5], it is difficult to understand the physiological mechanisms. Videofluoroscopic (VF) examination [6,7] is commonly used in research and clinical settings as the preferred standard method for assessing swallowing function because of the comprehensive information it provides. This method allows anatomic and kinematic analysis such as the movement of food bolus and swallowing-related organs. Videoendoscopic (VE) examination [8,9] is also widely used as a reliable and portable technique to observe the pharyngolaryngeal complex directly. However, the information on muscle activation patterns during swallowing cannot be obtained by these methods, though swallowing is controlled by the coordination of many muscles [5]. Surface electromyograms (sEMG) [10,11] are the best way to estimate muscle activation patterns non-invasively so far, but the simultaneous measurement of swallowing-related muscles is limited. The main reason for this is that most swallowing-related muscles are located deep below the surface and overlap as if forming a layered structure. As a result, sEMG cannot avoid cross-talk problems in the simultaneous measurement of many muscles in swallowing. Therefore, conventional methods cannot provide information to quantify the sequential pattern of the muscles in swallowing.

It is impossible to measure internal forces, such as joint contact forces and muscle strength, non-invasively with conventional techniques. Hence, biomechanical analysis using musculoskeletal models [12–15] has been considered as an alternative technique to estimate such internal forces. For example, musculoskeletal models for the lower extremities were used to analyze complicated inter-muscle coordination in dynamic movement, such as in walking [16,17], running [18], and jumping [19]. Upper extremity models [20,21] were also developed for the biomechanical analysis of dynamic motion of the upper limbs, such as in throwing [22], propelling of wheelchair [23], and so forth. Presently, large-scale musculoskeletal analysis is readily conducted, as software for developing a complicated musculoskeletal model has become available commercially [12,13] or as open-source software [14]. It may be expected that muscle activity during swallowing can be estimated in a similar manner as dynamic body movements even though most of the muscle activity involved in swallowing cannot be determined *in vivo*. However, there are few studies reporting musculoskeletal models of swallowing [24,25]. The authors have reported a musculoskeletal model of swallowing by analyzing normal swallowing motion considering muscle activity [26,27], but an analysis of details of the muscle activity in swallowing is still difficult and challenging.

Previous studies on computational biomechanical analysis of swallowing mainly focused on the interaction between the bolus and organs considering fluid dynamics [28–30]. In these studies, the deformation of organs was preliminarily provided by measured results and the activity of the muscles was not considered. However, estimating muscle activity would contribute to an understanding of the physiological aspects of swallowing as muscle expansion and contraction affect the deformation of organs.

This paper presents the design of a musculoskeletal model of swallowing and an investigation of muscle activity during pharyngeal swallowing. The skeletal model considers the hyoid bone and thyroid cartilage as a central element in the study of the swallowing function. The configuration of the swallowing-related muscles is defined based on anatomical knowledge, and the muscles are represented as a Hill-type model. The trajectories of the hyoid bone and thyroid cartilage using videofluoroscopic data of a healthy subject were analyzed for the dynamics' computations. The forces of individual muscles were estimated through inverse dynamics' computations with static optimization to study the activation pattern of the muscles and their contributions in the swallowing. The musculoskeletal

analysis is one method that can be used in the study of details of neuromuscular coordination of swallowing in future work.

2. Materials and Methods

2.1. Motion Analysis of the Hyoid Bone and Thyroid Cartilage during Swallowing

The normal swallowing process is generally classified into three phases according to the location of bolus: an oral phase, a pharyngeal phase, and an esophageal phase. The pharyngeal phase, where the bolus is transported from the pharynx into the esophagus, is especially important. Here, the larynx and pharynx move in a superior direction and the tongue base moves in a postero-superior direction in concert with movements of the hyoid bone and thyroid cartilage. As a result, the epiglottis folds down to prevent the bolus from entering the trachea leading it to the esophagus [31]. If this process is not completed fully, food and drink will enter the trachea and cause aspiration. Analyzing the movements of the hyoid bone and thyroid cartilage during the pharyngeal phase is important in the evaluation of swallowing because the movement of the larynx is affected by muscles attached to the hyoid bone and thyroid cartilage.

2.1.1. Method of the Analysis

To analyze two-dimensional movements of the hyoid bone and thyroid cartilage, we used an X-ray video (DR-2000F, Hitachi Medical Co., Tokyo, Japan) obtained from a videofluoroscopic (VF) examination, which recorded normal swallowing with a healthy, 25-year-old male who was not diagnosed with any other eating disorder or neurological diseases. Here, the volunteer swallowed 5 mL of water, including the contrast of $2.21 \times 10^{-6} \text{ m}^2/\text{s}$ viscosity, once. The volunteer gave his consent before the VF examination. The experimental procedure was approved by the ethics committee of Japanese Red Cross Musashino Hospital (No. 705). In the analysis, as shown in Figure 1, we manually extracted the region of the hyoid bone and the vocal ligament as the part of thyroid cartilage, frame by frame. The displacement and posture of each skeletal element were measured in relation to the initial position and orientation. Then, the measured displacements and postures were transformed to a global coordinate system with the center at the left–right occipital condyles. Each skeletal element has a local coordinate system at its center of gravity, as shown in Figure 1, and the volume of the two elements was estimated from skeletal data of a CT scan (Revolution CT, GE Healthcare Japan Co., Tokyo, Japan) of the same male. In the study here, the cricoid cartilage was included as part of thyroid cartilage.

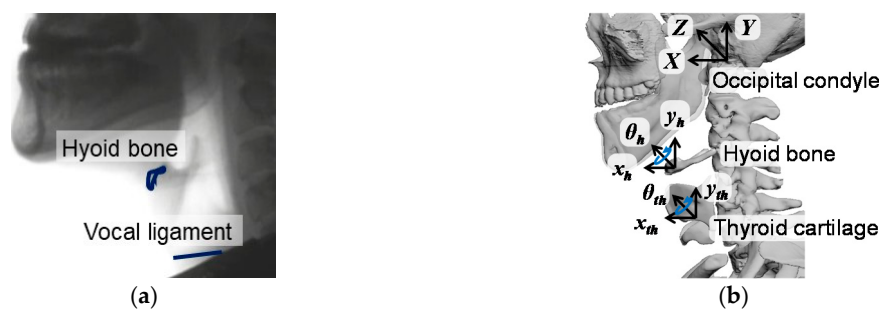


Figure 1. Trajectory analysis of the hyoid bone and thyroid cartilage. (a) Analyzed videofluoroscopic (VF) image, (b) global and local coordinate systems.

2.1.2. Results of the Analysis

Figure 2 shows the trajectories of the hyoid bone and thyroid cartilage in the sagittal plane, smoothed by a simple moving average. Figure 3 shows the displacements of the hyoid bone and thyroid cartilage in the X- and Y-axis directions, where P_s and P_e represent the starting and ending points, respectively. These figures show that the movements of the two elements can be divided into three phases. In the first phase, between P_s (0.90 s) and P_1 (1.36 s), the later oral phase, the hyoid bone

moves upward and slightly backward while thyroid cartilage moves upward and slightly forward. Here, the bolus is held in the oral cavity and its head reaches the soft palate. In the second phase, between P_1 and P_2 (1.73 s), the earlier pharyngeal phase, the two move together in an antero-superior direction and the soft palate is elevated. The bolus enters the oropharynx and the closure of the larynx by the epiglottis occurs. Then, the bolus moves to the hypopharynx and the esophagus. In the last phase, between P_2 and P_e (2.23 s), the later pharyngeal phase, they move in a postero-inferior direction to return to the resting positions, slightly different from the initial positions. The movement of the hyoid bone exhibits a typical triangular trajectory, as described in the literature [32].

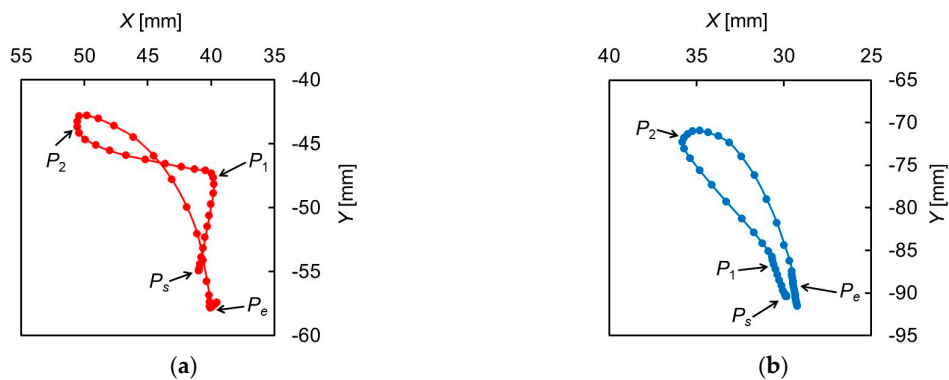


Figure 2. Trajectories of the hyoid bone and thyroid cartilage. (a) Hyoid bone, (b) thyroid cartilage.

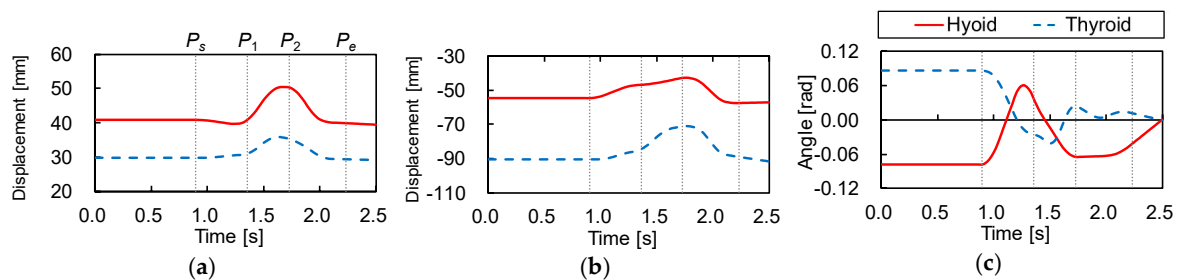


Figure 3. Displacements of the hyoid bone and thyroid cartilage. (a) Displacement in X-axis, (b) displacement in Y-axis, (c) rotation angle around Z-axis.

2.2. Development of the Musculoskeletal Model of Swallowing

2.2.1. Modeling of the Swallowing-Related Muscles

To analyze the muscle activity during swallowing, we developed a musculoskeletal model where a muscle is represented as an active constrictive wire actuator, by reference to the previous study [15]. In this model, the following 12 kinds of muscles were included as muscles acting on the hyoid bone and thyroid cartilage, as shown in Figures 4 and 5: the geniohyoid muscle, the stylohyoid muscle, the digastric muscle, the mylohyoid muscle, the sternohyoid muscle, the omohyoid muscle, the middle constrictor muscle, the thyrohyoid muscle, the sternothyroid muscle, the inferior constrictor muscle, the cricopharyngeus muscle, and the stylopharyngeus muscle. The muscles on the left and right sides are distributed symmetrically about the sagittal plane for simplicity. The origin and insertion of the muscles are shown in Table 1, defined based on anatomical description [33] and CT data in addition to BodyParts3D [34,35]. Broad muscles such as the mylohyoid and pharyngeal constrictor muscles are represented as multiple wires. Muscles with two muscle bellies such as the digastric and omohyoid muscles are modeled as two separate muscles with an intermediate tendon. The modeling of the musculoskeletal model was done using 3D modeling software, 3ds Max[®]. Further detailed description of the modeling of the swallowing-related muscles is as documented in previous studies [26,27].

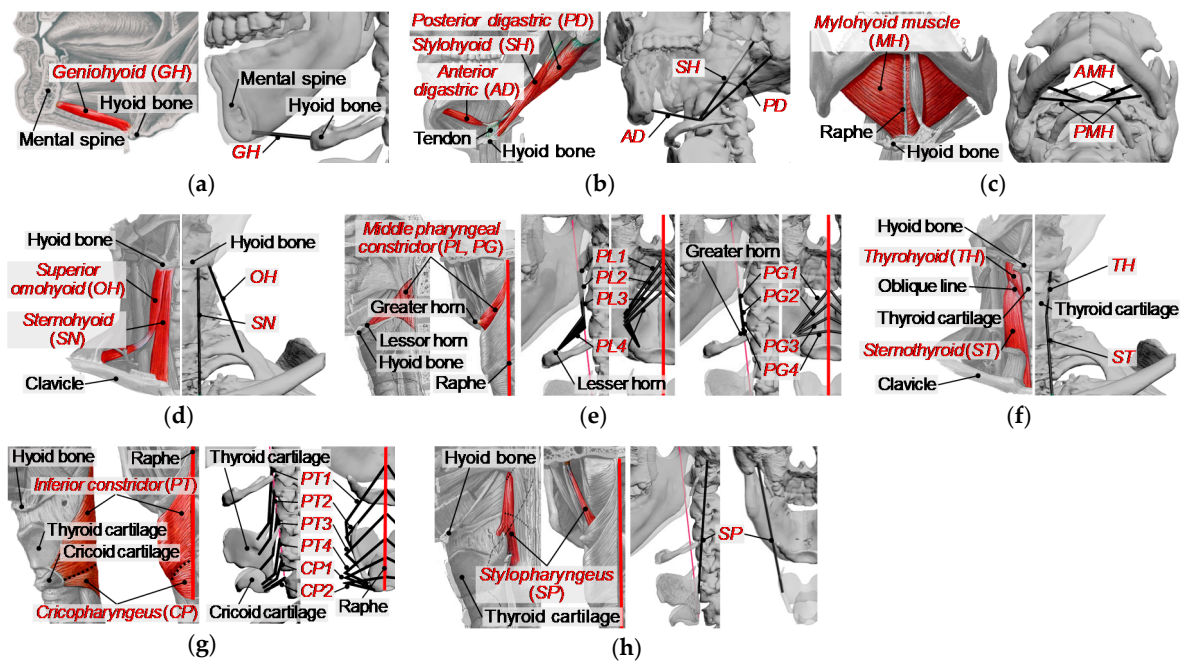


Figure 4. Swallowing-related muscles with wire models. Left image is an anatomical image of the muscle, and the wire model is shown on the right. (a) Geniohyoid (GH), (b) stylohyoid (SH) and digastric (AD, PD), (c) mylohyoid (AMH, PMH), (d) sternohyoid (SN) and omohyoid (OH), (e) middle pharyngeal constrictor (PG1-PG4, PL1-PL4), (f) thyrohyoid (TH) and sternothyroid (ST), (g) inferior pharyngeal constrictor (PT1-PT4) and cricopharyngeus (CP1, CP2), (h) stylopharyngeus (SP).

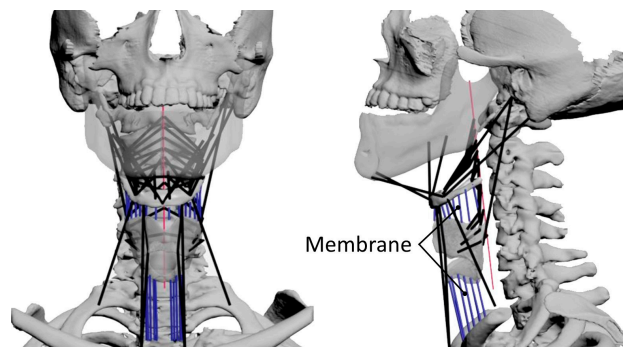


Figure 5. Overview of the musculoskeletal model of swallowing. The left image is a frontal view and the right image is a lateral view. The black lines represent muscle models and the blue lines represent membrane springs.

2.2.2. Modeling of Damping and Stiffness of Biological Tissue

To incorporate the viscous-elastic properties of biological tissue, such as skin, fat, muscle, membranes, and others, imaginary linear viscous and elastic components were added to constrain the movements of the hyoid bone and thyroid cartilage in the X- and Y-axis directions. However, it was quite difficult to represent the net effect accurately because the measurement of the complex mechanical properties of human soft tissue is not straightforward. Therefore, we assumed that the elastic constant of soft tissue for the movements in the X- and Y-axis directions was $k = 25.0 \text{ N/m}$ based on the previous study [36]. Then, the viscosity constant c was calculated to satisfy overdamping condition ($c > \sqrt{mk}$) due to high damping effect of the soft tissue. Here, m was the mass of the hyoid bone or thyroid cartilage. As a result, we assumed $c = 2.0 \text{ Ns/m}$.

Further, the thyrohyoid membrane between the hyoid bone and thyroid cartilage, as well as the membrane between the cricoid cartilage and trachea, were represented as multiple linear elastic

components. The elastic constant of each membrane component was experimentally defined as $k_m = 20.0 \text{ N/m}$ through an iterative process, so as to converge quadratic optimization program described below.

Table 1. List of swallowing-related muscles and their physiological cross-sectional areas (PCSAs).

Muscle Name	Symbol	Properties			
		Origin	Insertion	PCSA [$\times 10^{-6} \text{ m}^2$]	
Geniohyoid	GH	mental spine	anterior surface of the hyoid bone	4.60	
Stylohyoid	SH	posterior surface of the styloid process	lessor horn of the hyoid bone	2.70	
Digastric	anterior belly	AD	digastric fossa of the mandible	lessor horn of the hyoid bone	5.50
	posterior belly	PD	mastoid process	lessor horn of the hyoid bone	6.40
Mylohyoid	anterior part	AMH	anterior part of mylohyoid line	anterior surface of the hyoid bone	8.20
	posterior part	PMH	posterior part of mylohyoid line	anterior surface of the hyoid bone	4.30
Sternohyoid	SN	posterior part of the manubrium of sternum	lower border of the hyoid bone	3.41	
Omohyoid	superior belly	OH	intermediate tendon	lower border of the hyoid bone	2.75
	inferior belly	-	-	-	-
Middle pharyngeal constrictor	greater horn	PG1–4	greater horn of the hyoid bone	pharyngeal raphe	1.65 (*)
	lesser horn	PL1–4	lessor horn of the hyoid bone	pharyngeal raphe	1.13 (*)
Thyrohyoid	TH	oblique line on the thyroid cartilage	lower border of the hyoid bone	6.04	
Sternothyroid	ST	posterior part of the manubrium of sternum	oblique line on the thyroid cartilage	5.14	
Inferior pharyngeal constrictor	PT1–4	oblique line of thyroid lamina	pharyngeal raphe	2.25 (*)	
Cricopharyngeus	CP1, 2	rear part of cricoid	pharyngeal raphe	1.15 (*)	
Stylopharyngeus	SP	medial side of the styloid process	posterior border of the thyroid cartilage	1.90	

PCSA: Physiological cross-sectional area (*) represents the estimated value, which is not validated.

2.2.3. Modeling of the Mechanical Properties of Muscles

In swallowing, the hyoid bone and thyroid cartilage are mainly moved by a tug-of-war among the muscles, and the passive force of a muscle generated when it is stretched in addition to the active contractile force must be considered. The Hill-type muscle model [37], which is commonly used in musculoskeletal studies, was used as a simple phenomenological computational model to represent the mechanical properties of the muscles in this study.

The Hill-type muscle model consists of a contractile element (CE), a parallel spring element (PE), and a serial spring element (SE). The capacity to generate the force of a muscle is defined by the force-length and force-velocity properties of the contractile element and the nonlinear spring properties of the passive elements. The total muscle force is the sum of the active (F_{ce}) and passive forces (F_{pe}) as below:

$$F_{mus} = F_{ce} + F_{pe}. \tag{1}$$

As reported elsewhere [38,39], the active force generated by the contractile elements can be described by the following Equations (2) and (3):

$$F_{ce}(a, l_{ce}, \dot{l}_{ce}) = a f_{lce}(l_{ce}) f_{vce}(\dot{l}_{ce}) \cos(\alpha) f_{max} \tag{2}$$

$$f_{max} = \sigma_{max} PCSA \tag{3}$$

where a is the level of activation of a muscle ranging from 0 and 1, $f_{lce}(l_{ce})$ represents the relationship between the normalized muscle force and its length, $f_{vce}(\dot{l}_{ce})$ represents the relationship between the normalized muscle force and its contractile velocity, α is the pennation angle of the muscle, σ_{max} is the maximum isometric muscle stress, and $PCSA$ is the physiological cross-sectional area of the muscle. The force-length relationship, $f_{lce}(l_{ce})$, shows a Gaussian distribution around the optimal muscle fiber length l_{ce0} as below:

$$f_{lce}(l_{ce}) = \exp\left[-\left(\frac{l_{ce} - l_{ce0}}{l_{cesh}}\right)^2\right]. \tag{4}$$

Here, l_{ce} and l_{ce0} are the current and optimal lengths of a contractile element and l_{cesh} is a parameter defining the shape of the Gaussian force-length curve. Note that the optimal length l_{ce0} was assumed as the muscle length in the resting state in this study. The force-velocity relationship, $f_{vce}(\dot{l}_{ce})$, is formulated as follows:

$$f_{vce}(\dot{l}_{ce}) = \begin{cases} 0 & (\dot{l}_{ce} \leq -v_{max}) \\ \frac{V_{sh}(v_{max}(a, l_{ce}) + \dot{l}_{ce})}{V_{sh}v_{max}(a, l_{ce}) - \dot{l}_{ce}} & (-v_{max} \leq \dot{l}_{ce} < 0) \\ \frac{V_{sh}V_{shl}v_{max}(a, l_{ce}) + V_{ml}\dot{l}_{ce}}{V_{sh}V_{shl}v_{max}(a, l_{ce}) + \dot{l}_{ce}} & (\dot{l}_{ce} \leq 0) \end{cases} \tag{5}$$

$$v_{max}(a, l_{ce}) = V_{vm}\{1 - V_{er}[1 - af(l_{ce})]\} \tag{6}$$

where v_{max} is the maximum contractile velocity of the muscle without load, and the muscle contractile velocity slows as the load increases; V_{sh} and V_{shl} are parameters defining the concavity of the Hill curve during shortening and lengthening, respectively; V_{ml} and V_{vm} are the maximum velocities during concentric contraction and during maximum isometric contraction, respectively; and V_{er} is the effect of the activation on the maximum velocity.

The passive force-length relationship of a muscle is represented by an exponential function as below:

$$F_{pe}(l_{mus}) = \begin{cases} 0 & (l_{mus} \leq l_{mus0}) \\ \frac{F_{max}}{e^{PE_{sh}}}\left(e^{\frac{l_{mus} - l_{mus0}}{l_{mus0}} \cdot \frac{PE_{sh}}{PE_{xm}}} - 1\right) & (l_{mus} > l_{mus0}) \end{cases} \tag{7}$$

with PE_{sh} and PE_{xm} as the shape and range parameters of the passive force and l_{mus} and l_{mus0} as the current and optimal muscle lengths. The parameter values of the muscles in this study were defined by referring to previous work [38,39], as shown in Table 2.

2.2.4. Physiological Cross-Sectional Area (PCSA)

The physiological cross-sectional area (PCSA) is used to estimate the maximum muscle force because the maximum muscle force is related to PCSA. Table 1 shows the PCSA of swallowing-related muscles included in the musculoskeletal model, which were defined based on the results of physiological studies [40–42]. However, the PCSA of pharyngeal constrictor and cricopharyngeus muscles (PG, PL, PT, and CP) were estimated based on BodyParts3D [34,35] in addition to anatomical images [33] as these values were not investigated in the previous work. Here, we calculated the PCSAs of pharyngeal constrictor muscles based on their 3D polygon data using 3D modeling software, 3ds Max®.

Table 2. Parameters of the muscle model.

Parameter	Value	Unit
σ_{max}	0.7×10^6	[N/m ²]
l_{mus0}	Derived from the model	[m]
l_{ce0}	l_{mus0}	[m]
l_{cesh}	$0.5l_{ce0}$	[m]
V_{vm}	$6l_{ce0}$	[m/s]
V_{sh}	0.3	[-]
V_{shl}	0.23	[-]
V_{ml}	1.3	[-]
V_{er}	0.2	[-]
PE_{sh}	4.0	[-]
PE_{xm}	0.4	[m]

2.2.5. Muscle Force Estimation Using an Optimization Program

(1) Equation of Motion

Using Lagrangian mechanics and setting the generalized coordinates as q , the dynamic equations (such as Equation (8)) of the musculoskeletal model in the following form were obtained:

$$M\ddot{q} + C\dot{q} + Kq + F_{pa}^m + g(q) = Q \tag{8}$$

where M is the inertia matrix with a mass M and a moment of inertia J and C and K are damping and stiffness matrices, respectively. The F_{pa}^m is the matrix representing the passive force of the muscles. The matrix g represents the effect of gravity. The $q = [x^h, y^h, z^h, \theta^h, x^{th}, y^{th}, z^{th}, \theta^{th}]^T$ stands for positions and postures of the hyoid bone and thyroid cartilage. The $Q = [F_x^h, F_y^h, F_z^h, T^h, F_x^{th}, F_y^{th}, F_z^{th}, T^{th}]^T$ is the generalized force, which includes forces and torques acting on the hyoid bone and thyroid cartilage. The h and th indices stand for parameters related to the hyoid bone and thyroid cartilage, respectively. The mass of the hyoid bone and thyroid cartilage, M^h and M^{th} , were estimated to be 5.0×10^{-3} kg and 1.5×10^{-2} kg, respectively, by calculating the volumes from the skeleton data. Further, the moment of inertia about the center of gravity of the hyoid bone and thyroid cartilage, J^h and J^{th} , were estimated using the function of 3D CAD software, SolidWorks®, to be 4.12×10^{-7} kg m² and 2.92×10^{-6} kg m², respectively.

Using the dynamic Equation (8), inverse dynamics analysis was performed to compute the generalized force Q incorporating the forces and torque that realize the motion of the hyoid bone and thyroid cartilage, as shown in Figure 2. Here, the differentiation of q with time was computed by a finite-difference method. In addition, the effect of gravity was eliminated ($g = 0$) for simplicity.

(2) Muscle Force Estimation

The developed musculoskeletal model has a redundant number of muscles compared with the degrees of freedom of the hyoid bone and thyroid cartilage. Due to this redundancy, estimating the muscle forces from the obtained generalized forces was an ill-posed problem, and to solve it, Crowninshield’s cost function $O(f)$ [16] was used. The function was formed as a quadratic program as below:

$$O(f) = \sum_{i=1}^N \left(\frac{f_i}{PCSA_i} \right)^2 \rightarrow \min \tag{9}$$

$$\text{subject to : } F_x = \sum_{i=1}^N f_{ix}, \quad F_y = \sum_{i=1}^N f_{iy}, \quad T_\theta = \sum_{i=1}^N f_i r_i \tag{10}$$

$$f_i^{min} \leq f_i \leq f_i^{max} \quad (i = 1, \dots, N) \tag{11}$$

where $PCSA_i$ is the physiological cross-sectional area (PCSA) of the muscle i , f_i is the muscle force, r_i is the moment arm of muscle i at the hyoid bone or thyroid cartilage, f_i^{max} is the maximum force of the muscle i , and f_i^{min} is the minimum. A combination of possible muscle forces that minimize the total muscle force was obtained by optimizing the cost function (9). Function (10) is the equality constraint and possible muscle forces were required to satisfy the forces and the torque computed by inverse dynamics. Possible muscle forces were also constrained to be equal to or above zero by the inequality constraint (11) because muscles generate only contractile force. Here, f_i^{max} was calculated for each muscle by Equation (3) and f_i^{min} was zero ($f_i^{min} = 0$). The quadratic program was solved using MATLAB® function.

3. Results

3.1. Results of Muscle Force Estimation

Figure 6 shows the muscle forces ($\%F_{max}$) estimated by the inverse dynamics computation of swallowing and the static optimization, which were normalized by the maximum forces as below:

$$\%F_{max} = \frac{f_e}{f_{max}} \quad (12)$$

where f_e and f_{max} are the estimated force and the maximum force of muscle, calculated by Equations (3) and (9), respectively. The figure also shows the three characteristic points defined in Figure 2 to compare the muscle activities with the movements of the hyoid bone and thyroid cartilage. Figure 7 shows the onset and duration of the muscle activity, which was derived from Figure 6. The activation level was defined as values higher than 1% of the maximum force, and the contrast coloring changed depending on the muscle force. The results suggest which muscle mainly contributes to swallowing, and they confirmed that the activities of the muscles correlate with the movements of the hyoid bone and thyroid cartilage.

Figures 2, 6 and 7 show that all suprahyoid muscles (PMH, AMH, GH, AD, PD, and SH) and an upper part of the middle pharyngeal constrictor muscle (PG1) begin to generate contractile forces to pull the hyoid bone in the postero-superior direction in the first phase between P_s and P_1 . Here, ST also contributes a counterbalancing force to the thyroid cartilage, preventing it from being pulled in the posterior direction by the passive force of TH and thyrohyoid membrane, which are stretched. SP seems to contribute to maintaining the posture of thyroid cartilage in this period. In the second phase, between P_1 and P_2 , GH, AD, PD, and SH generate larger forces to move the hyoid in an antero-superior direction. Here, TH, SP, and a part of inferior pharyngeal constrictor (PT1 and PT2) begin to generate force to pull the thyroid upward and slightly forward. After reaching the maximum displacement at 1.73 s, in the last phase between P_2 and P_e , the later pharyngeal phase, the activation of all muscles are declined, and the hyoid bone and thyroid cartilage return to the resting position by the passive forces of the stretching muscles and membranes.

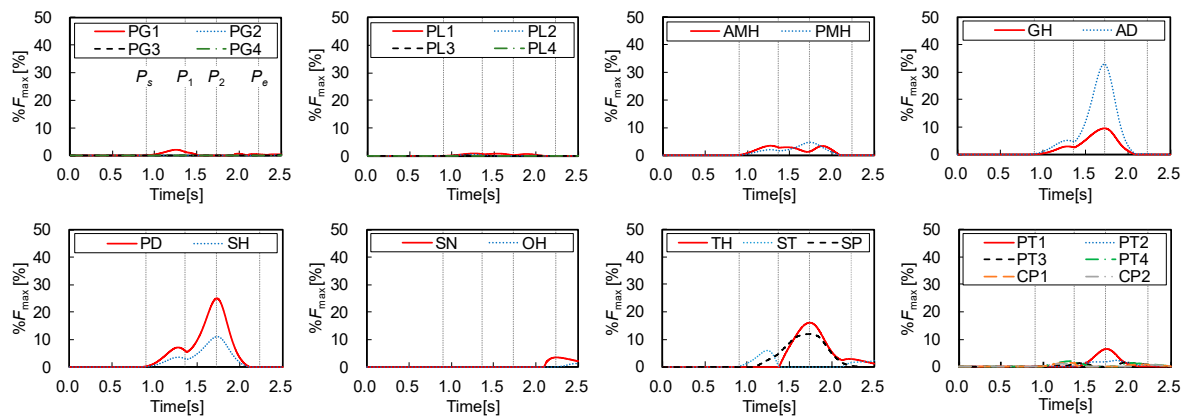


Figure 6. Estimated results of time changes in muscle forces.

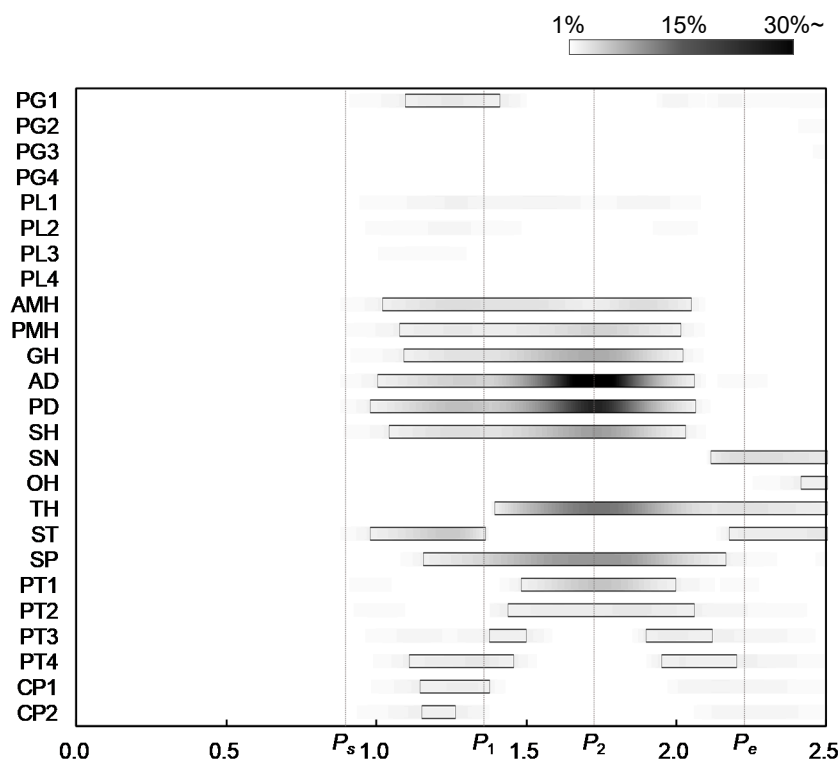


Figure 7. Onsets and durations of activity of swallowing-related muscles.

3.2. Force Direction of the Muscles

The hyoid bone and thyroid cartilage mainly move in anterior and superior directions, as shown in Figure 2. Therefore, to calculate the maximum contraction forces of the muscles in the anterior-posterior direction and the superior-inferior direction, it is important to investigate the role of each muscle in the movements of the hyoid bone and thyroid cartilage. Figure 8 shows the direction of the maximum contractile force of each muscle in the anterior-posterior and superior-inferior directions, which were calculated from Figure 6.

From Figure 8, the contribution is large in order of AD and GH in pulling the hyoid bone in the anterior direction. For thyroid cartilage, only TH contributes in the anterior movement. In the same manner, the contribution is large in order of PD, SH, PMH, AMH, GH, and AD in elevating the hyoid bone. For the superior movement of thyroid, the contribution order is TH, SP, and PT1.

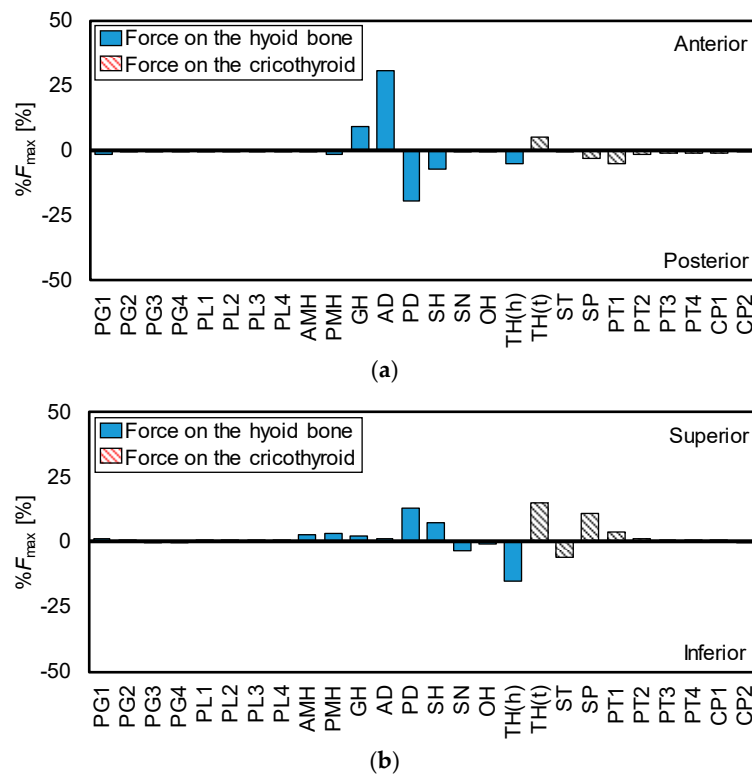


Figure 8. Ratios and directions of maximum force of each muscle. (a) Anterior-posterior, (b) superior-inferior.

4. Discussion

4.1. Activity Pattern of the Muscles

The major contribution of this study was to estimate the sequential activation pattern of the many muscles involved in swallowing based on the dynamics of swallowing, which is hard with conventional methods. In the same manner, the estimated activation pattern can be divided into three phases, corresponding to the sequence of events in swallowing. In the first time period, P_s-P_1 , the later oral phase, most of the suprahyoid muscles and a part of middle pharyngeal constrictor muscles are activated to elevate the hyoid bone to push the tongue against the hard palate to hold bolus. The result indicates that PMH, AMH, GH, AD, PD, and SH contribute to elevating the hyoid bone and, particularly, PD and SH make significant effort. Subsequently, in the second period, P_1-P_2 , the early pharyngeal phase, those muscles are more activated to move the hyoid bone anteriorly and superiorly, in which GH and AD show a remarkable contribution to the anterior movement. In addition, TH, SP, and PT1 are activated to raise thyroid cartilage slightly behind the hyoid bone. In the third period, P_2-P_e , the later pharyngeal phase, all the muscles tend to relax, returning the hyoid bone and thyroid cartilage to resting positions. During the pharyngeal phase, the larynx rises along with the antero-superior movements of the hyoid bone and thyroid cartilage, and the epiglottis folds backward to cover the entrance of the larynx to keep bolus from entering windpipe. At the same time, the pharynx would extend to transport bolus into the esophagus.

To estimate the muscle activity, electromyography (EMG) was conventionally used as a reliable technique. In particular, fine wire EMG was widely used to evaluate swallowing-related muscles individually and to investigate sequential muscle activation patterns [43–48]. In these previous studies, activities of typical muscles involved in swallowing were investigated, but not the deep muscles, which are difficult to approach by wire electrode. The following findings were obtained:

- Some studies have indicated that activation of AD, GH, MH, and SN varied with food characteristics and that there were no obvious consistent activation patterns [43–45]. However, a more recent study suggested that there was a typical sequence of muscle activation [46]. That is, the masseter (MA) is first, the next is GH and AD, and the last is SN.
- SN was rarely activated or showed quite low values in comparison with the other muscles [43,46].
- The onset of muscle activation of MH before that of TH was significant [47].
- Normal activity of CP exhibits an inhibition phase in swallowing: Preswallowing and rebound bursts across the pause [48].

Similar findings were also observed in this study. That is, GH and AD are activated at an early stage in addition to MH (AMH, PMH), PD, and SH to move the hyoid bone anteriorly and superiorly. The onset of MH (AMH, PMH) precedes the activation of TH, which mainly contributes to the movement of thyroid cartilage, and the activity of SN is quite low. Besides, CP (CP1, CP2) and the lower region of PT (PT3, PT4) slightly exhibited twice activation. However, note that the number of muscles that can be measured by conventional methods are limited, unlike our approach.

4.2. Role of the Muscles

Figure 8 reveals the role of each muscle in the movements of the hyoid bone and thyroid cartilage. The figure shows the reasonable result, that is, all suprahyoid muscles (AMH, PMH, GH, AD, PD, and SH) contribute to the superior movement of the hyoid bone because they are located above the hyoid bone. Similarly, it is understandable that GH and AD show the most effort in the anterior movement of the hyoid bone as they are in front of the hyoid bone. TH dominantly works on the thyroid movements and it is estimated to exert the largest force in the anterior-superior movement of thyroid cartilage. Meanwhile, TH also contributes to depressing the hyoid bone as it is located between the hyoid bone and thyroid cartilage.

To understand how the muscle morphological properties influence hyoid movement, Pearson et al. [41] investigated muscle attachment sites, and physiological cross-sectional areas (PCSA) of the suprahyoid muscle subsamples (the geniohyoid muscle, stylohyoid muscle, digastric muscle, and mylohyoid muscle) were investigated by an anatomical technique. They evaluated the potential effect of individual muscles on the hyoid bone using the PCSA forces of the muscles. The PCSA force, which represents the strength of the muscles in the anterior-posterior direction or the superior-inferior direction, was calculated from the attachment sites and PCSA of the muscles. As the result, it predicted that GH and MH have the most potential to affect the anterior and superior displacement of the hyoid bone, respectively, which is partially consistent with the findings derived from this study. In addition, our research emphasizes the importance of suprahyoid muscles in terms of swallowing dynamics.

4.3. Limitations

The findings of this study considering the dynamics of swallowing were consistent with the results of previous studies based on physiological measurement and structural analysis. However, there were some limitations to this study. First, the analysis was of only one healthy young volunteer. Even though the movement of the hyoid bone of the volunteer is a typical triangular trajectory, to generalize the results it would be better to increase the number of volunteers of various ages and genders because hyoid movement is slightly varied among individuals. In particular, to investigate the effects of aging is important, as muscle strength weakens with age and swallowing disorders are common in the elderly. Second, in relation to the first, we developed the musculoskeletal model using the CT data of the young volunteer, but the skeleton geometry also differs among individuals and that difference influences the dynamics calculation. Thus, a deformable standard skeleton model is required to represent different genders and ages. Besides, to analyze the sensitivity of subject-specific modeling to the uncertainties in the identification of muscle attachment site, muscle-tendon parameters and stiffness parameters of soft tissues are interesting because the geometry of head and neck parts is varied

among individuals. Third, there are some simplifications. The effect of tongue deformation done by tongue muscles was not accurately simulated but it actually affects the kinematics and posture of the hyoid bone. Similarly, linear elastic and viscous behaviors were assumed for soft tissues surrounding the hyoid bone and thyroid cartilage. Thus, nonhomogeneity and anisotropy of their restrictions were not taken into account. In addition, the inertial effect of the muscles on the movements of the hyoid and thyroid was not considered, because Hill-type muscle model does not include muscle mass. However, the inertia of the attached muscles cannot be ignored as their masses are actually larger than that of the hyoid bone and thyroid. To overcome these simplifications, a 3D, finite element model of muscle and soft tissue should be constructed based on physiological literature. The 3D musculoskeletal model would also enable us to take into account the interaction between muscles and the effect of gravity on muscle deformation. Fourth, there are some assumptions and hypothesis due to the lack of physiological data. Most of the PCSA of the muscles derived from cadaver specimens was used as that of the young volunteer and the PCSA of the pharyngeal constrictor muscles were estimated from a 3D anatomical model. In addition, the estimated muscle forces in this study may not be a unique combination, because the estimated result depended on the objective function of the optimization process. Although the objective function considered physiological properties of muscles and is widely accepted in musculoskeletal studies, its general applicability is not fully accepted. Thus, the results of this study should be validated further by physiological manner.

To investigate muscle activities in swallowing is difficult because swallowing is a complex behavior involving volitional and reflexive activities of many nerves and muscles. In general, EMG measurements are recognized as a reliable method to estimate muscle activities. At the same time, however, there are limitations in measuring deep muscles in the neck even with fine wire electrodes. Further, EMG signals do not necessarily reflect muscle strength. In comparing with EMG measurement, the advantage of the proposed method is that it is able to estimate muscle strengths that can satisfy dynamic consistency parameters with the movement of the hyoid bone and thyroid cartilage calculated using VF images, and as the activities of deep muscles can be estimated. As a result, this technique is only one method to investigate individual muscles in swallowing. If the musculoskeletal analysis of swallowing were validated physiologically, this technique would be useful for swallowing rehabilitation. For example, it may extract the target muscle group, which has to be recovered to obtain the desired therapeutic effect. Another possible application is to propose effective postural compensation maneuver for swallowing safely without aspiration.

5. Conclusions

A musculoskeletal model was developed, with the main muscles around the hyoid bone and thyroid cartilage included, to study the muscle activity during swallowing. The forces of individual muscles between the later oral phase and the pharyngeal phase of normal swallowing of a healthy volunteer were estimated by inverse dynamics computations with a static optimization technique. The predicted muscle activation patterns showed qualitative agreement with salient features obtained from previous studies. This study shows that the musculoskeletal analysis has the potential to provide deeper insight into swallowing mechanism than conventional methods in terms of swallowing dynamics.

One of our future works is to implement a muscle model with volume like finite element method (FEM) to investigate the effects of deformation of muscle, tongue, and soft tissues on the movements of the hyoid and thyroid. Although the Hill-type muscle model does not have volume, the effect of muscle deformation cannot be ignored in swallowing as the hyoid and thyroid are held by the muscles. Besides, to integrate simulation models of tongue deformation [29,30] and mastication [49], it is also important to analyze the coordination of mastication and swallowing.

Author Contributions: Conceptualization, T.H., T.K. (Takahiro Kikuchi), and Y.M.; methodology, T.H. and A.M.; software, T.H., A.M., F.C.-S., and M.U.; data acquisition, T.K. (Takahiro Kikuchi) and Y.M.; writing—original draft preparation, T.H.; writing—review and editing, M.U., T.K. (Takahiro Kikuchi), and Y.M.; supervision,

T.K. (Takuji Koike); funding acquisition, T.H. All authors have read and agreed to the published version of the manuscript.

Funding: This research was funded by JSPS KAKENHI Grant Numbers 18K09706 and 19K22980 and Tateishi Science and Technology Foundation.

Conflicts of Interest: The authors declare no conflict of interest.

References

1. Statistics Bureau of Japan. Current Population Estimates as of 1 October 1 2016. Available online: <http://www.stat.go.jp/english/data/jinsui/2016np/index.htm> (accessed on 1 March 2017).
2. Statistics and Information Department Minister's Secretariat of Ministry of Health, Labour and Welfare. Vital Statistics of Japan 2015—Trends in Leading Causes of Death: Japan. Available online: <http://www.e-stat.go.jp/SG1/estat/ListE.do?lid=000001158057> (accessed on 1 March 2017).
3. Teramoto, S.; Fukuchi, Y.; Sasaki, H.; Sato, K.; Sekizawa, K.; Matsuse, T. High incidence of aspiration pneumonia in community- and hospital-acquired pneumonia in hospitalized patients: A multicenter, prospective study in Japan. *J. Am. Geriatr. Soc.* **2008**, *56*, 577–579. [[CrossRef](#)] [[PubMed](#)]
4. Kaplan, V.; Angus, D.C.; Griffin, M.F.; Clermont, G.; Watson, R.S.; Linde-Zwirble, W.T. Hospitalized Community-acquired Pneumonia in the Elderly Age- and Sex-related Patterns of Care and Outcome in the United States. *Am. J. Respir. Crit. Care Med.* **2002**, *165*, 766–772. [[CrossRef](#)]
5. Cunningham, E.T., Jr.; Jones, B. Anatomical and Physiological Overview. In *Normal and Abnormal Swallowing: Imaging in Diagnosis and Therapy*, 2nd ed.; Jones, B., Ed.; Springer: New York, NY, USA, 2003; pp. 11–34.
6. Palmer, J.B.; Kuhlemeier, K.V.; Tippett, D.C.; Lynch, C. A protocol for the videofluorographic swallowing study. *Dysphagia* **1993**, *8*, 209–214. [[CrossRef](#)] [[PubMed](#)]
7. Scharitzer, M.; Pokieser, P. Videofluoroscopy: Current Clinical Impact in Deglutology. *J. Gastroenterol. Hepatol. Res.* **2014**, *3*, 1061–1065.
8. Leder, S.B.; Sasaki, C.T.; Burrell, M.I. Fiberoptic endoscopic evaluation of dysphagia to identify silent aspiration. *Dysphagia* **1998**, *13*, 19–21. [[CrossRef](#)] [[PubMed](#)]
9. Aviv, J.E.; Kaplan, S.T.; Thomson, J.E.; Spitzer, J.; Diamond, B.; Close, L.G. The Safety of Flexible Endoscopic Evaluation of Swallowing with Sensory Testing (FEESST): An Analysis of 500 Consecutive Evaluations. *Dysphagia* **2000**, *15*, 39–44. [[CrossRef](#)]
10. Neis, L.R.; Logemann, J.; Larson, C. Viscosity effects on EMG activity in normal swallow. *Dysphagia* **1994**, *9*, 101–106.
11. Crary, M.A.; Baldwin, B.O. Surface Electromyographic Characteristics of Swallowing in Dysphagia Secondary to Brainstem Stroke. *Dysphagia* **1997**, *12*, 180–187. [[CrossRef](#)]
12. Delp, S.T.; Loan, J.P. A computational framework for simulating and analyzing human and animal movement. *IEEE Comput. Sci. Eng.* **2000**, *2*, 46–55. [[CrossRef](#)]
13. Damsgaard, M.; Rasmussen, J.; Christensen, S.T.; Surma, E.; de Zee, M. Analysis of musculoskeletal systems in the AnyBody Modeling System. *Simul. Model. Pract. Theory* **2006**, *14*, 1100–1111. [[CrossRef](#)]
14. Delp, S.L.; Anderson, F.C.; Arnold, A.S.; Loan, P.; Habib, A.; John, C.T.; Guendelman, E.; Thelen, D.G. OpenSim: Open-source software to create and analyze dynamic simulations of movement. *IEEE Trans. Biomed. Eng.* **2007**, *54*, 1940–1950. [[CrossRef](#)] [[PubMed](#)]
15. Nakamura, Y.; Yamane, K.; Fujita, Y.; Suzuki, I. Somatosensory Computation for Man-Machine Interface from Motion Capture Data and Musculoskeletal Human Model. *IEEE Trans. Robot.* **2005**, *21*, 58–66. [[CrossRef](#)]
16. Crowninshield, R.D.; Brand, R.A. A physiologically based criterion of muscle force prediction in locomotion. *J. Biomech.* **1981**, *14*, 793–801. [[CrossRef](#)]
17. Ravera, E.P.; Crespo, M.J.; Braidot, A.A. Estimation of muscle forces in gait using a simulation of the electromyographic activity and numerical optimization. *Comput. Methods Biomech. Biomed. Eng.* **2014**, *19*, 1–12. [[CrossRef](#)] [[PubMed](#)]
18. Sasaki, K.; Neptune, R.R. Muscle mechanical work and elastic energy utilization during walking and running near the preferred gait transition speed. *Gait Posture* **2006**, *23*, 383–390. [[CrossRef](#)] [[PubMed](#)]
19. Anderson, F.C.; Pandy, M.G. A Dynamic Optimization Solution for Vertical Jumping in Three Dimensions. *Comput. Methods Biomech. Biomed. Eng.* **1999**, *2*, 201–231. [[CrossRef](#)]

20. Holzbaur, K.R.S.; Murray, W.M.; Delp, S.L. A Model of the Upper Extremity for Simulating Musculoskeletal Surgery and Analyzing Neuromuscular Control. *Ann. Biomed. Eng.* **2005**, *33*, 829–840. [[CrossRef](#)]
21. Nikooyan, A.A.; Veeger, H.E.J.; Chadwick, E.K.J.; Praagman, M.; Helm, F.C. Development of a comprehensive musculoskeletal model of the shoulder and elbow. *Med. Biol. Eng. Comput.* **2011**, *49*, 1425–1435. [[CrossRef](#)]
22. Lin, H.T.; Nakamura, Y.; Su, F.C.; Elias, J.J.; Hashimoto, J.; Chao, E.Y.S. Use of Virtual, Interactive, Musculoskeletal System (VIMS) in Modeling and Analysis of Shoulder Throwing Activity. *J. Biomech. Eng.* **2005**, *127*, 525–530. [[CrossRef](#)]
23. Sasaki, M.; Stefanov, D.; Ota, Y.; Miura, H.; Nakayama, A. Shoulder joint contact force during lever-propelled wheelchair propulsion. *Robomech J.* **2015**, *2*, 1–10. [[CrossRef](#)]
24. Stavness, I.; Hannam, A.G.; Lloyd, J.E.; Fels, S. An Integrated Dynamic Jaw and Laryngeal Model Constructed from CT Data. In Proceedings of the Third International Symposium for Biomedical Simulation, Zurich, Switzerland, 10–11 July 2006; pp. 169–177.
25. Hannam, A.G.; Stavness, I.; Lloyd, J.E.; Fels, S. A dynamic model of jaw and hyoid biomechanics during chewing. *J. Biomech.* **2008**, *41*, 1069–1076. [[CrossRef](#)] [[PubMed](#)]
26. Hashimoto, T.; Murakoshi, A.; Kikuchi, T.; Michiwaki, Y.; Koike, T. Development of musculoskeletal model for the hyoid bone during swallowing. In Proceedings of the 2016 IEEE-EMBS International Conference on Biomedical and Health Informatics, Las Vegas, NV, USA, 24–27 February 2016; pp. 457–460.
27. Hashimoto, T.; Murakoshi, A.; Kikuchi, T.; Michiwaki, Y.; Koike, T. Development of Musculoskeletal Model to Estimate Muscle Activities during Swallowing. In *Digital Human Modeling: Applications in Health, Safety, Ergonomics and Risk Management (Lecture Note in Computer Science)*; Duffy, V.G., Ed.; Springer: Cham, Switzerland, 2016; Volume 9745, pp. 82–91.
28. Sonomura, M.; Mizunuma, H.; Numamori, T.; Michiwaki, H.; Nishinari, K. Numerical simulation of the swallowing of liquid bolus. *J. Texture Stud.* **2011**, *42*, 203–211. [[CrossRef](#)]
29. Ho, A.K.; Tsou, L.; Green, S.; Fels, S. A 3D swallowing simulation using smoothed particle hydrodynamics. *Comput. Methods Biomech. Biomed. Eng. Imaging Vis.* **2014**, *2*, 237–244. [[CrossRef](#)]
30. Kikuchi, T.; Michiwaki, Y.; Kamiya, T.; Toyama, Y.; Tamai, T.; Koshizuka, S. Human swallowing simulation based on videofluorography images using Hamiltonian MPS method. *Comput. Part. Mech.* **2015**, *2*, 247–260. [[CrossRef](#)]
31. Pearson, W.G.; Taylor, B.K.; Blair, J.; Martin-Harris, B. Computational analysis of swallowing mechanics underlying impaired epiglottic inversion. *Laryngoscope* **2016**, *126*, 1854–1858. [[CrossRef](#)]
32. Ishida, R.; Palmer, J.B.; Hiiemae, K.M. Hyoid Motion during Swallowing: Factors Affecting Forward and Upward Displacement. *Dysphagia* **2002**, *17*, 262–272. [[CrossRef](#)]
33. McFarland, D.H. *Netter's Atlas of Anatomy for Speech, Swallowing, and Hearing*, 2nd ed.; Elsevier—Health Sciences Division: Amsterdam, The Netherlands, 2008; pp. 109–170.
34. BodyParts3D/Anatomography. Available online: <http://lifesciencedb.jp/bp3d/> (accessed on 1 March 2019).
35. Mitsuhashi, N.; Fujieda, K.; Tamura, T.; Kawamoto, S.; Takagi, T.; Okubo, K. BodyParts3D: 3D structure database for anatomical concepts. *Nucleic Acids Res.* **2009**, *37* (Suppl. 1). [[CrossRef](#)]
36. Pailler-Mattei, C.; Bee, S.; Zahouani, H. In vivo measurements of the elastic mechanical properties of human skin by indentation test. *Med. Eng. Phys.* **2008**, *30*, 599–606. [[CrossRef](#)]
37. Hill, A.V. The heat of shortening and the dynamic constants of muscle. *Proc. R. Soc. Lond. Ser. B Biol. Sci.* **1938**, *126*, 136–195.
38. Strove, S. Learning combined feedback and feedforward control of a musculoskeletal system. *Biol. Cybern.* **1996**, *75*, 73–83. [[CrossRef](#)]
39. Strove, S. Impedance Characteristics of a Neuromusculoskeletal model of the human arm I. Posture Control. *Biol. Cybern.* **1999**, *81*, 475–494. [[CrossRef](#)]
40. Borst, J.; Forbes, P.A.; Happee, R.; Veeger, D.H. Muscle parameters for musculoskeletal modelling of the human neck. *Clin. Biomech.* **2011**, *26*, 343–351. [[CrossRef](#)]
41. Pearson, W.G., Jr.; Langmore, S.E.; Zumwalt, A.C. Evaluating the Structural Properties of Suprahyoid Muscles and their Potential for Moving the Hyoid. *Dysphagia* **2011**, *26*, 345–351. [[CrossRef](#)] [[PubMed](#)]
42. Pearson, W.G., Jr.; Langmore, S.E.; Yu, L.B.; Zumwalt, A.C. Structural Analysis of Muscles Elevating the Hyolaryngeal Complex. *Dysphagia* **2012**, *27*, 445–451. [[CrossRef](#)] [[PubMed](#)]
43. Palmer, J.B.; Rudin, N.J.; Lara, G.; Crompton, A.W. Coordination of Mastication and Swallowing. *Dysphagia* **1992**, *7*, 187–200. [[CrossRef](#)] [[PubMed](#)]

44. Spiro, J.; Rendell, J.; Gay, T. Activation and coordination patterns of the suprahyoid muscles during swallowing. *Laryngoscope* **1994**, *104*, 1376–1382. [[CrossRef](#)]
45. Palmer, P.M.; McCulloch, T.M.; Jaffe, D.; Neel, A.T. Effects of a Sour Bolus on the Intramuscular Electromyographic (EMG) Activity of Muscles in the Submental Region. *Dysphagia* **2005**, *20*, 210–217. [[CrossRef](#)]
46. Inokuchi, H.; González-Fernández, M.; Matsuo, K.; Brodsky, M.B.; Yoda, M.; Taniguchi, H.; Okazaki, H.; Hiraoka, T.; Palmer, J.B. Electromyography of Swallowing with Fine Wire Intramuscular Electrodes in Healthy Human: Activation Sequence of Selected Hyoid Muscles. *Dysphagia* **2014**, *29*, 713–721. [[CrossRef](#)]
47. Burnett, T.A.; Mann, E.A.; Stoklosa, J.B.; Ludlow, C.L. Self-Triggered Functional Electrical Stimulation during Swallowing. *J. Neurophysiol.* **2005**, *94*, 4011–4018. [[CrossRef](#)]
48. Perlman, A.L.; Palmer, P.M.; McCulloch, T.M.; Vandaele, D.J. Electromyographic activity from human laryngeal, pharyngeal, and submental muscles during swallowing. *J. Appl. Physiol.* **1999**, *86*, 1663–1669. [[CrossRef](#)]
49. Rohrlea, O.; Pullana, A.J. Three-dimensional finite element modelling of muscle forces during mastication. *J. Biomech.* **2007**, *40*, 3363–3372. [[CrossRef](#)] [[PubMed](#)]



© 2020 by the authors. Licensee MDPI, Basel, Switzerland. This article is an open access article distributed under the terms and conditions of the Creative Commons Attribution (CC BY) license (<http://creativecommons.org/licenses/by/4.0/>).